A Geometrical Method for the Analysis of Simulation Bundles

Rodrigo Iza-Teran[1] and Jochen Garcke[1,2]

[1]Fraunhofer SCAI, Sankt Augustin
[2]Institut für Numerische Simulation, Universität Bonn

October 27, 2017

Abstract

In a development process using computer-aided engineering, changes to initial conditions are usually studied, which gives rise to large and complex data stemming from the numerical solution of partial differential equations. We propose a new data analysis approach for the efficient post-processing of the resulting bundles of finite element data.

Our analysis approach is based on the mathematical principles of symmetry. We assume that a set of transformations exists, albeit unknown, which map simulation to simulation. In particular, we consider the case where simulations of an industrial product are assumed to be contained in the space of surfaces embedded in $\mathbb{R}^3$. In this setting a discrete Laplace-Beltrami operator can be constructed on the mesh, which is invariant to isometric transformations and therefore valid for all simulations. The eigenfunctions of such an operator are used as a common basis for all (isometric) simulations. To extend the idea of invariance to other transformations, we propose the use of an operator that can be constructed for a stochastic setting. A result from nonlinear independent component analysis allows us to construct a discrete Fokker-Planck operator that in the continuous limit converges to an operator invariant to a nonlinear transformation.

Two remarkable properties are observed numerically, namely that the coefficients obtained by projecting the simulation to the orthogonal basis from both operators decay very fast, and that at each level of the eigendecomposition, the eigenvectors are seen to recover different independent variation modes like rotation, translation or local deformations. Theoretical results about the decay of the spectral coefficients, as well as the recovery of independent variations are presented for the stochastic case.

We use numerical simulations of car crashes as our data source for the examples. For these time dependent datasets, we show that only a few spectral coefficients are necessary to describe the data variability. Low dimensional structures are obtained in this way, which are able to capture information about the underlying simulation space, in particular an analysis for many simulations in time is made possible. The introduced data analysis approach therefore allows an effective analysis of the complex data from many numerical simulations.

1 Introduction

In computer-aided engineering (CAE) one models the physical behavior of industrial products by partial differential equations (PDEs), which are then solved numerically. Nowadays the art of simulation is highly developed in several industries, where high performance computer systems

are used to solve finite element models for many design variants. Therefore, engineers need to analyze and compare a large number of simulations in the product development process, with the goal to get the best product performance, while taking functional constraints, costs, or regulations into account.

Today in industry, a large amount of engineering know-how and time is invested for the evaluation of model variants based on corresponding numerical simulations. Their detailed investigation involves time dependent 3D visualization of the simulated product, e.g. in the form of movements or deformations, but analyzing and trying to identify cause and effect using the full finite element mesh—in the range of millions of nodes—is a challenging task. Due to the difficulty of comparing very fine discretization meshes, usually only a few derived scalar quantities, such as energy absorption or deformations in selected points of the structure, or performance curves, e.g. vibration response curves, are used for the evaluation of the simulation results.

In this work, we introduce a novel analysis approach, which can efficiently compare 3D finite element mesh data and therefore overcome the outlined challenge. The motivation and idea for our method are inspired by the notion of symmetry as used for the analytical solution of differential equations. Since numerical simulations are solutions of partial differential equations, they can be analysed under the mathematical principle of symmetry. This is in the sense that one can apply a transformation to one simulation, and that the object after the transformation cannot be distinguished from the original one in the underlying mathematical space; in other words, it is invariant to the transformation. Finding such a transformation for a specific realistic situation as modeled by a PDE is clearly difficult. Nevertheless, if available, such transformation would be sending all simulations to an invariant space, so we could instead focus on such a space directly. We show realistic situations, where it is indeed possible to find ways to obtain a representation in a suitable invariant space, which captures part of the inherent symmetry.

As an example consider deformations of a car structure, which are modeled as (thick) surfaces. In many practical cases, the variations between different simulations, e.g. due to changes in the material parameters, are distance preserving, which means that after a deformation the distance between points inside the geometric structure stays the same. Instead of looking for a transformation directly, we propose to look for a differential operator which observes suitable invariance properties. For isometric transformations of a surface, the Laplace-Beltrami operator is such an invariant operator, which one can approximate for the discrete surface using graph distances on the mesh. Now, if we assume that all simulations are obtained through such a transformation, the operator will be kept the same. Since this operator is positive semidefinite, its spectral orthogonal decomposition can be obtained and an orthogonal basis of an invariant space can be constructed. In other words, an equivalent representation of the space, invariant to isometric changes, can be built. One now can project mesh functions, in particular those from the simulation results, into the new basis for the invariant space, the obtained spectral coefficients represent a set of equivalent, but transformed simulations.

In the case of crash simulations, car parts are surfaces embedded in $\mathbb{R}^3$, so the space of all possible isometric deformations is big. But, as we project them to the invariant basis, a natural decomposition is obtained along sets of equivalent classes, where different type of orbits are obtained tracing the space of all isometric deformations. An intuitive analogy provides the case of the sphere, where the orbits are circles with varying radius. Joining all such circles will in the end recover the full sphere. Projecting a set of isometric deformations to an orthogonal basis produces exactly the desired partitioning. In the end, one just has to consider the spectral coefficients along the different components of the orthogonal decomposition, they represent the orbits. As we will see, the number of basis elements in the new representation can be high, i.e. the number of nodes of the discrete mesh, nevertheless we observe empirically for realistic simulation data that these coefficients decay very fast; only few of them are large and reflect the variability

of the simulations. Furthermore, an interesting observation is that we can identify specific independent physical effects, which are represented by components of the spectral decomposition, e.g. independent isometric variations such as translations, rotations, or deformations.

Besides the discrete Laplace-Beltrami operator, we alternatively use a discrete Fokker-Planck operator, whose construction comes from nonlinear independent component analysis [SC08]. Here, we assume that a numerical simulation is the combined result of deterministic effects and nonlinear stochastic Itô processes per mesh point. From the observed simulations we can construct a discrete operator, which in the continuous limit converges to a Fokker-Planck operator, which is invariant to the nonlinear transformation by the deterministic effects. Two important consequences of the analysis in [SC08] are, first, that a separation along the independent components is achieved by the eigenfunctions of the operator and, second, that such a decomposition rewrites the original problem as a superposition of 1D Sturm-Liouville eigenproblems, in particular with a large decay of the spectral coefficients in the case of smooth functions.

In summary, the high dimensional simulation data can be transformed into a compact representation by using eigenvectors of suitable operators, enabling not only an efficient dimensionality reduction, but also simplifying further analysis tasks. We employ two different operators, one respecting isometric transformations and one built from the observed data to be invariant to an underlying nonlinear transformation.

We start with a summary of related research in section 2. The mathematical setting is presented in section 3, while in section 4 we consider the Laplace-Beltrami operator and a specific Fokker-Planck operator connected to stochastic Itô processes, as well as their discrete versions. First results when projecting several simulations to the eigenvectors of these operators are presented in section 5, together with a theoretical observation about the decay of the spectral coefficients as well as the obtained separation of independent isometric components. A data analysis approach is proposed in section 6 and we apply the method to an industrial engineering application in section 7.

2 Related Work

Considering related research for the analysis of data from numerical simulations in engineering, a common approach is the so-called sensitivity analysis. In its simplest form, one input variable is varied at a time, scalar output quantities of interest are evaluated for a few simulation results and sensitivity is measured by linear regression. Extensions are available in several ways, in particular in the form of response surface approaches [MMAC09], where the most relevant quantities of interest are trained as fitted functions of the input parameters, based on the results of a few numerical simulations. The underlying assumption is that the information content of all simulations can be concentrated in the scalar quantities of interest. This is also the major drawback of this approach, it fails when the relation between input parameters and the overall behavior of the simulation cannot be reduced to such scalar quantities, or is not well understood, e.g. due to complicated nonlinear behavior.

In contrast to sensitivity analysis, we aim to look at the data in more detail and work with the full numerical simulation data, here only limited research happened so far. One of the first works analyzing engineering data from full numerical simulations was [AGHH08], where the authors used principal component analysis (PCA) for detecting important parameters from nonlinear finite element simulations. Car crash simulations where analyzed in [MT08] using clustering with a local distance measure, where regions of similar deformation behavior were identified and evaluated with this approach. The PCA has also been used in [TNNC10] for a group of simulations where some parameters have been changed, the approach uses the first eigenvectors

of the covariance matrix of all given simulations as deformation modes.

While linear methods such as the PCA have proven to be successful for industrial applications, it is nevertheless known that if nonlinear correlations are present in the data, the use of the PCA is not optimal, see e.g. [LV07]. In [BGIT+13] several nonlinear methods from machine learning have been used for the analysis of crash simulations. Good reconstruction capabilities using a nonlinear principal manifold approach were shown, as well as the detection of the principal effects and their dependencies on input variables by using diffusion maps. Additionally, [Iza14] shows the application of diffusion maps to the analysis of engineering data in crash simulation, vibration analysis, and metal forming. The approach was able to cluster deformation data and vibration curves from simulation bundles, showing that the most important input variable changes can be expressed using clusters in low dimensional embeddings.

Additionally, we refer to the related areas of statistical shape analysis and 3D geometry analysis. Here theoretical work has been done in the area of statistical shape analysis, where statistics on shape manifolds, e.g. intrinsic and extrinsic means, are studied. Started by the work of Kendall [KBCL99], this is a very active research area, recent work can for example be found in [SJML05, FJ07, HHM10] and the references therein. A fundamental difference to methods applied in manifold learning is that in shape analysis a manifold structure of the shape space is supposed to be known and is kept fixed. Additionally, we would like to mention the area of Riemannian geometries for plane curves and surfaces [MM06, BHM11], those papers, and several others referenced therein, illustrate the way to the definition of an abstract mathematical setting for those spaces, that likely can be extended to the analysis of the space of simulations.

Finally, we mention 3D geometry analysis, where the study object is a surface mesh embedded in $\mathbb{R}^3$. A number of methods have been developed for pose independent shape classification [LSS+10], shape retrieval [RWP06], shape segmentation [RBG+09], invariant mesh representation [LSLCO05], and compression [BCG05], to name a few. Many of these applications make use of the Laplace-Beltrami operator specially for pose independent processing, that is, if two shapes are isometric, i.e. geodesic distances are preserved, then ideally a method will not distinguish between them. Note that this is exactly the opposite of what we want, we would like to distinguish between two isometrically deformed shapes since they are the result of a simulation with different input parameters. We also mention [OBCS+12], where 3D shapes are compared assuming the existence of an a-priori known transformation bringing one shape into another. While this has a connection to our approach, it is substantially different since it describes a shape using features which are then used for classification or pose independent shape matching. As will be seen, our approach can be interpreted expressing the same shape in another coordinate system. The intention of our approach is not to improve 3D shape analysis methods, but to be able to classify, reconstruct, and explore simulation data during the design of new products.

3 Mathematical Setting

We give in this section a review of the mathematical setting, in particular Riemannian manifolds, which in our case reduces to being quotient spaces of manifolds by isometric group actions. We shortly consider a space of simulations and describe the discrete setting for surface approximation.

3.1 Riemannian Manifolds and Quotient Spaces

Let us start with some definitions from differential geometry, for details refer to, e.g., [Mic08]. Let φ be a diffeomorphism $\varphi : \mathcal{M} \to \mathcal{M}'$ between two Riemannian manifolds $(\mathcal{M}, g)$ and $(\mathcal{M}', g')$ with $g = \varphi^* g'$, where the pullback of g' by φ is defined by $\varphi^* g' = g' \circ \varphi$. If we have $d_{g'}(\varphi(p), \varphi(q)) =$

$d_g(p,q)$, where d_g is induced by the metric tensor g, we call φ (geodesic) distance preserving or an isometry.

Consider a Riemannian manifold $(\mathcal{M}, g)$ and a function $f \in C^\infty(\mathcal{M})$, $f : \mathcal{M} \to \mathbb{R}$. Using concepts such as differential maps, exterior derivatives and k-forms, one can naturally define the gradient $\nabla_g f$ and the divergence div_g. Furthermore, the Laplace-Beltrami operator $\Delta_g : C^\infty \to C^\infty$ on a manifold is defined as $\Delta_g = -\mathrm{div}_g \cdot \nabla_g$. Note that in the following we will denote d_g on $\mathcal{M}$ by $d_\mathcal{M}$, and correspondingly Δ_g by $\Delta_\mathcal{M}$, since the specific metric tensor is not of interest.

The flexibility of constructing topological spaces can be enhanced through the use of equivalence relations, i.e. a relation on $\mathcal{M} \times \mathcal{M}$ that satisfies transitivity, reflexivity and symmetry properties. Elements of $\mathcal{M}$ that satisfy an equivalence relation form a quotient space.

For our purposes we consider special type of quotient spaces, namely those constructed using a group G acting on $\mathcal{M}$. As a reminder, given a group G and a set $\mathcal{M}$, a group action is a map $G \times \mathcal{M} \to \mathcal{M}$ written as $(a, p) \rightarrowtail a \cdot p$ that satisfies the axioms of identity and compatibility. If a group G acts on a space $\mathcal{M}$ by homeomorphism, then we have the orbit equivalence relation: $x \sim y$ if and only if $x = a \cdot y$ for some $a \in G$. Formally, given a group G acting on $\mathcal{M}$, an orbit of a point x in $\mathcal{M}$ is the set of elements of $\mathcal{M}$ to which x can be moved by the elements of G. Formally for $x \in \mathcal{M}$, the orbit of x is defined as

$$[x] = \{a \cdot x \in \mathcal{M} \,|\, a \in G\}\,.$$

The set of all orbits is called orbit space and is written as $\mathcal{M}/G$.

3.2 Solution Space of Simulations

We want to study the space of time dependent (numerical) solutions of a partial differential equation on a given fixed domain Ω, where the variations are obtained by changing boundary and/or initial conditions. Simulations are numerical solutions of partial differential equations and in this work we assume they are surfaces or surface functions embedded in $\mathbb{R}^3$. To formulate the underlying abstract setting, which motivates our data analysis approach, we make the following two assumptions:

- Each solution at a given time is a (Riemannian) 2-manifold $\mathcal{M}$ embedded in $\mathbb{R}^3$.
- Numerical solutions are obtained by group transformations, which in particular are assumed to be isometries, i.e. at each time step a solution $\mathcal{M}^i$ is isometric to an initial, or reference, manifold $\mathcal{M}$.

We propose to treat numerical simulation results as shapes and consider the Riemannian framework that has been developed for shape spaces, see [MM06, BHM11, BBM14]. According to this framework, the shape space is a quotient space of a manifold modulo a group action G over it. For simulations we would then use, under the assumptions above, the space of orbits

$$Emb(\mathcal{M}, \mathbb{R}^3)/G(\mathcal{M}),$$

where $Emb(\mathcal{M}, \mathbb{R}^3)$ is the set of embeddings of $\mathcal{M}$ in $\mathbb{R}^3$ and G is the group of transformations that leave a surface invariant with respect to distances as measured in the reference surface $\mathcal{M}$.

Which particular structure a specific simulation space has, will depend on the type of transformation group G. Rotations, translations and deformations are examples of transformation groups which arise in our application. A particular case, the space $Emb(\mathcal{M}, \mathbb{R}^3)/Diff(\mathcal{M})$ has been studied intensively in [MM06, BHM11, BBM14] in the more general context of embeddings in $\mathbb{R}^n$ modulo the action of the group of diffeomorphism $Diff(M)$, they are shown to be special

manifolds. In these references the case of immersions in $\mathbb{R}^n$ is also treated; those spaces are in the above references shown to be of so-called orbifold type (due to the presence of singularities). For more details about this setting for simulations see [Iza17].

3.3 Discrete Setting

We view the discretization of a solution of a PDE as a mesh approximation K of a 2-manifold $\mathcal{M}$, which is isometrically embedded in $\mathbb{R}^3$. The following definition is one way to quantify how well a mesh K approximates a manifold $\mathcal{M}$, see [BSW08] for details.

Definition 3.1. *Let K be a meshed surface approximating $\mathcal{M}$, where the vertices of K are on $\mathcal{M}$. We say that K is an (ϵ, η)-approximation of $\mathcal{M}$ if the following two conditions are fulfilled:*

- *For a face t in K, the maximum distance between any two points on t is at most $\epsilon\rho$, where ρ is the* reach*, defined as the infimum of the local distance between any point w in $\mathcal{M}$ and the medial axis of the surface $\mathcal{M}$.*
- *For a face t in K and a vertex $p \in t$, the angle between n_t, the unit outward normal of the plane passing through t, and n_p, the unit outward normal of $\mathcal{M}$ at p, is at most η.*

Furthermore, we have restrictions of continuous functions on $\mathcal{M}$ to the mesh K:

Definition 3.2. *Let $f : \mathcal{M} \to \mathbb{R}$ be a continuous function on $\mathcal{M}$. The function f evaluated at the nodes of a mesh K is called a mesh function $f|_K : K \to \mathbb{R}$.*

In the following we use f to denote both, the continuous function on $\mathcal{M}$ and its restriction to K.

4 Discrete Representations of Operators On Manifolds

We consider the important component of our approach, namely the use of so called invariant differential operators, which have a special behavior under isometric transformations, and establish discrete approximations for such operators.

4.1 Laplace-Beltrami Operator

For the Laplace-Beltrami operator $\Delta_{\mathcal{M}} := \Delta_g|_{\mathcal{M}}$ we consider the eigenvalue problem $\Delta_{\mathcal{M}}\psi = -\lambda\psi$, restricted to the manifold $(\mathcal{M}, g)$, where λ is an eigenvalue of $\Delta_{\mathcal{M}}$ and ψ is the corresponding eigenfunction. Here we point also to the classic relation between the Laplace operator and Fourier analysis, which is an underlying them of the following. We have a positive semidefinite operator, therefore all eigenvalues λ_j, $j \geq 0$ are real, positive, and isolated with finite multiplicity. The set of normalized eigenfunctions $\{\psi_j\}_{j=1}^{\infty}$ of the operator forms an orthonormal basis for functions on $\mathcal{M}$, therefore the following decomposition can be written for $f \in C^{\infty}(\mathcal{M})$:

$$f = \sum_{j=0}^{\infty} \alpha_j \psi_j, \quad \alpha_j = \langle f, \psi_j \rangle_g. \tag{1}$$

For any function f as defined in (1) one can, instead of considering the function itself, equivalently consider its vector of spectral coefficients $\alpha = [\alpha_1, \alpha_2, ...]$, obtained by projecting the function along the infinite dimensional eigenspace spanned by the eigenfunctions. Those coefficients can be used to compute the distance of functions due to the Parseval identity as follows:

Proposition 4.1. *The difference between two functions f^1, f^2, with $f^i = \sum_{j=0}^{\infty} \alpha_j^i \psi_j$, $\alpha_j^i = \langle f^i, \psi_j \rangle$, $\alpha^i = [\alpha_1^i, \alpha_2^i, \ldots]$, $i = 1, 2$, using a decomposition with the corresponding normalized eigenfunctions for an operator $\Delta_g(\mathcal{M})$, is given by*

$$\|f^1 - f^2\|^2 = \sum_{i,j=0}^{\infty} \langle (\alpha_i^1 - \alpha_i^2)\psi_i, (\alpha_j^1 - \alpha_j^2)\psi_j \rangle^2 = \|\alpha^1 - \alpha^2\|^2.$$

4.1.1 The Laplace-Beltrami Operator on a Mesh

Let $\mathcal{M}$ be as before a surface, i.e. a 2-manifold isometrically embedded in $\mathbb{R}^3$. Let K be an (ϵ, η)-approximation of $\mathcal{M}$. Further, let t be a face in K, let $\#t$ denote the number of vertices on t, and let $V(t)$ be the set of vertices of t. Then, for any vertex $w \in V(t)$ of any face $t \in K$, following [BSW08] a mesh Laplace operator can be defined as

$$L_K^h f(w) = \frac{1}{4\pi h^2} \sum_{t \in K} \frac{Area(t)}{\#t} \sum_{p \in V(t)} e^{-\frac{d(p,w)^2}{4h}} (f(p) - f(w)), \tag{2}$$

where h is a parameter which corresponds to the size of the local neighborhood at a point and $d(p, w)$ denotes the graph distance, i.e. the length of the shortest path between p and w along the graph, using Euclidean distances between the vertices as graph weights.

In the following theorem one exploits that the Euclidean distance is locally a good approximation of the geodesic distance and obtains an approximation result for the Laplace-Beltrami operator $\Delta_{\mathcal{M}}$ on a surface $\mathcal{M}$ by the mesh Laplace operator L_K^h on a corresponding mesh K.

Theorem 4.2. (Laplace-Beltrami Approximation Theorem [BSW08]) *Let $K_{\epsilon,\eta}$ be a an (ϵ, η)-approximation of $\mathcal{M}$. Put $h(\epsilon, \eta) = \epsilon^{\frac{1}{2.5+\alpha}} + \eta^{\frac{1}{1+\alpha}}$ for an arbitrary positive number $\alpha > 0$. Then for any function $f \in C^2(\mathcal{M})$ it holds*

$$\lim_{\epsilon,\eta \to 0} \sup_{K_{\epsilon,\eta}} \left\| L_{K_{\epsilon,\eta}}^{h(\epsilon,\eta)} f - \Delta_{\mathcal{M}} f|_{K_{\epsilon,\eta}} \right\|_{\infty} = 0,$$

where the supremum is taken over all (ϵ, η)-approximations of $\mathcal{M}$.

Notice that in [BSW08] the Euclidean distance $\|p - w\|$ is used in the definition of L_K^h instead of $d(p, w)$. Since the graph distance is for an (ϵ, η)-approximation of $\mathcal{M}$ a better approximation of the geodesic distance than the Euclidean distance, the theorem naturally holds for definition (2) as well. According to this result, for a mesh fine enough which also approximates the curvature of $\mathcal{M}$ well, we expect to get an approximation of the corresponding continuous Laplace-Beltrami operator on this surface.

4.1.2 The Laplace-Beltrami Operator under Isometric Transformations

We are now given a discrete surface mesh K that approximates a surface $\mathcal{M}$. Further let φ^i be a distance preserving diffeomorphism $\varphi^i : \mathcal{M} \to \mathcal{M}^i$ between two Riemannian manifolds $(\mathcal{M}, g)$ and $(\mathcal{M}^i, g^i)$ and let $\bar{K} = \left\{K^i\right\}_{i=1}^m$ be a set of meshes which are assumed to have the same connectivity and approximate a set of φ^i transformed surfaces $\mathcal{M}^i$, $i = 1, \ldots, m$. The transformation is such that geodesic distances are kept the same, i.e. φ^i is an isometry. Then $\mathcal{M}, \mathcal{M}^i$ are called isometric and the restriction to the discrete mesh are assumed to preserve geodesic distances as well. In this ideal case the following diagram commutes.

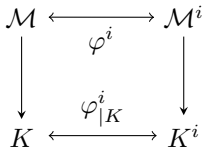

Here $\varphi^i_{|K}$ is a discrete version of φ^i, i.e. vertices are mapped to vertices.

Notice that in a discrete setting it is a-priori not clear how to handle geodesic distance preservation. In general, an error is made by an approximate computation of geodesic distances and one assumes that this error is kept small. In particular, we assume that a point on a mesh is sampled from the surface and that we approximate the geodesic distance by using the graph distance on the mesh. The discrete nature of the mesh results in an approximation to the geodesic distance on the surface, in particular for an (ϵ, η)-approximation of $\mathcal{M}$ the difference between geodesic and graph distance can be made arbitrarily small with decreasing ϵ and η, see [Iza17] for details and proof.

Generally, one can describe the behavior using the concept of ε-isometry, where given two manifolds $\mathcal{M}, \mathcal{M}'$, a transformation $\varphi : \mathcal{M} \mapsto \mathcal{M}'$ is said to be an ε-isometry if

$$\sup_{p,w \in \mathcal{M}} |d_{\mathcal{M}}(p, w) - d_{\mathcal{M}^i}(\varphi(p), \varphi(w))| \leq \varepsilon.$$

We now assume that the discrete transformations $\varphi^i_{|K}$ are ε-isometric between (discrete) surfaces. Assuming a Gaussian distribution on the error, we can state the following on the effect of an error in the distances on the corresponding discrete Laplace-Beltrami operator.

Proposition 4.3. *1) Let a surface $\mathcal{M}$ be given and let a geodesic distance preserving mapping φ^i transform $\mathcal{M}$ into a series of deformed surfaces $\mathcal{M}^i$, $i = 1, \ldots, m$. The Laplace-Beltrami operator constructed using the geodesic distance in $\mathcal{M}$ is the same as the one for each $\mathcal{M}^i$.*

2) Let the set of meshes $\bar{K} = \left\{K^i\right\}_{i=1}^m$ contain the approximations of the surfaces $\mathcal{M}^i$ and let there be transformations $\varphi^i_{|K}, i = 1, \ldots, m$ between the meshes which are ε-isometric, where the ε will depend on the two respective meshes involved. Further, assume that the ε-isometric transformations produce a Gaussian noise perturbation of the metric. Then, the approximation of the Laplace-Beltrami operator L^h_K given in (2), constructed using graph distances for one mesh K, differs only by a scaling factor from the ones constructed using one of the deformed meshes $i = 1, \ldots, m$ in the set $\bar{K}$.

Proof sketch. The first statement is obvious, since the geodesic distance stays the same after an isometric transformation, calculating the Laplace-Beltrami operator based on it will lead to the same result.

For the second statement we are in the discrete case, so the geodesic distance is approximated by the graph distance, where we assume a small error perturbation of magnitude ϵ which follows a Gaussian distribution. Now, we can use a result from [EK10], which states that for the Gaussian kernel, as we use here, such a Laplacian matrix disturbed by noise can be considered a rescaled version of the original one. For the full proof see [Iza17]. □

These considerations justify that the simulation bundle can be jointly projected into the eigenbasis obtained from one discrete operator. We make use of expression (2), evaluated on a reference mesh. The graph distance, as an approximation of the geodesic distance, is calculated using the algorithm described in [MMP87]. To approximate the Laplace-Beltrami operator (2) we use a slightly modified version of the software[1] used in [BSW08]. That algorithm requires a

[1] J. Sun, MeshLP: Approximating Laplace-Beltrami Operator from Meshes, `geomtop.org/software/meshlp`

parameter $\rho \cdot \sqrt{h}$ which controls the maximum geodesic distance of nodes which are employed in the calculation of a matrix entry. The overall procedure is described in algorithm 1.

Algorithm 1: Spectral decomposition of the discrete Laplace-Beltrami operator

Input: simulation x^r: a triangular mesh in $\mathbb{R}^3$ with N_h points and N_f faces
Parameter: ρ, h, p
Output: first p eigenvectors of the discrete Laplace-Beltrami operator

foreach $\tilde{k} \in \{1, \ldots, N_f\}$ **do** ▷ `estimate areas of each face`
  foreach $i \in \{1, 2, 3\}$ **do** ▷ `1/3 of area assigned to each vertex`
    $area[\tilde{k}_i] = (\text{area of face } \tilde{k})/3$ ▷ `face` $\tilde{k}$ `vertices indexed by` $\tilde{k}_i$
foreach $k \in \{1, \ldots, N_h\}$ **do** ▷ `weight matrix with graph distances`
  $[ids, dists] = \text{graphdist}(k, x^r, \rho \cdot \sqrt{h})$ ▷ `distances on` x^r `up to` $\rho \cdot \sqrt{h}$
  foreach $l, d \in [ids, dists]$ **do**
    $\mathbf{W}[k, l] = area[k] \cdot area[l] \cdot \exp(-d^2/(4h))/(4\pi h^2)$
$\mathbf{L} = \mathbf{W} - \mathbf{D}$, where $\mathbf{D} = diag(\mathbf{W} \cdot \mathbb{1})$ ▷ `compute graph Laplacian`
decompose $\mathbf{L}$ by $[\mathbf{U}, \mathbf{E}] = \text{EVD}(\mathbf{L})$ ▷ `non-trivial eigenvectors`
return first p non-trivial eigenvectors $\mathbf{U}$

4.2 Fokker-Planck Operator

In addition to the use of the Laplace-Beltrami operator, operators with other types of invariances are possible. We now introduce a specific Fokker-Planck operator, which is based on ideas developed in the context of nonlinear independent component analysis (NICA) [SC08, KHC12]. The underlying model for the data assumes independent stochastic Itô processes $p^{(i)}$ which are given by

$$dp^{(i)} = \alpha^i(p^{(i)})dt + b^i(p^{(i)})dw^i, \ i = 1, \ldots N_h,$$

where α^i and b^i are unknown drift and noise coefficients, and $\dot{w}^i$ are independent white noises, i.e. the w^i are Wiener processes. One assumes that an observation of the N_h-dimensional process $p = (p^{(1)}, p^{(2)}, \ldots, p^{(N_h)})$ is not possible, but that the result of a (nonlinear) mapping $\varphi : \mathcal{S}^p \to \mathcal{S}^\eta$ is available.

Let us connect this to the analysis of simulations in engineering, as an example we consider again crash simulations for cars. In the industrial design work flow, for a given set of design parameters a numerical simulation is performed observing the equations of structural mechanics and computing deformations over time. For a fixed time step, we can interpret the deformed mesh as the result of a mapping φ from the initial mesh. Now, besides the deterministic laws of structural mechanics, there are additional stochastic or uncertain effects. These might be due to (random) variations of the design parameters, as is the case for reliability design or robustness studies, due to numerical errors or instabilities, due to uncertainties in the modeling assumptions, e.g. the material models or parameters, or other effects. In other words, the numerical result at a given time step is the result of deterministic effects—modeled by the mapping φ—and stochastic effects, modeled by a stochastic Itô processes $p^{(i)}$ per mesh point. Surely, whether the assumption of underlying Itô processes, and in particular their independence, is valid for this practical setting is rather speculative, but note that there are approaches in structural dynamics that use this assumption, see e.g. [CP94] for the Itô formulation characterizing accumulated structural deformations. We conjecture, that at least for small time steps, the variation in the

numerical results due to variations in material parameters can be viewed in a stochastic setting, while the independence should be viewed in an approximate fashion.

We now sketch results from [SC08, KHC12], which allow an approximate distance computation in the unobservable space $\mathcal{S}^p$ by using data samples in the observable space $\mathcal{S}^\eta$. Given N_h points $p^{(1)}, \cdots, p^{(N_h)} \in \mathbb{R}^M$ in the unobservable space $\mathcal{S}^p$, they are mapped to points $\eta^{(1)}, \cdots, \eta^{(N_h)} \in \mathbb{R}^d$ in another space $\mathcal{S}^\eta$ by a nonlinear transformation φ, i.e. $\eta^{(k)} = \varphi(p^{(k)})$. Considering a Taylor series of the inverse φ^{-1} at $(\eta^{(k)} + \eta^{(l)})/2$, one can derive linear approximations to $p^{(k)}$ and $p^{(l)}$ and estimate their Euclidean distance by

$$\|p^{(k)} - p^{(l)}\|^2_{\mathbb{R}^M} = (\eta^{(k)} - \eta^{(l)})^T \left[(J_\varphi J_\varphi^T)^{-1} \left(\frac{\eta^{(k)} + \eta^{(l)}}{2} \right) \right] (\eta^{(k)} - \eta^{(l)}) + O(\|\eta^{(k)} - \eta^{(l)}\|^4_{\mathbb{R}^d}).$$

While we do not have access to J_φ, one can write the local covariance matrix of an observed process using Itô's lemma as

$$C = J_\varphi J_\varphi^T,$$

and one can compute a sample covariance $C^{(l)}$ as an approximation from the observed data. Finally, since $(J_\varphi J_\varphi^T)^{-1}$ at $(\eta^{(k)} + \eta^{(l)})/2$ cannot be obtained that way, a second order approximation of it is employed by averaging $(J_\varphi J_\varphi^T)^{-1}(\eta^{(k)})$ and $(J_\varphi J_\varphi^T)^{-1}(\eta^{(l)})$ and taking the inverse. We summarize this approximation in the following proposition, see [SC08, KHC12] for details.

Proposition 4.4. *Let $p, p' \in \mathcal{S}^p \subset \mathbb{R}^M$, and let η, η' be their respective mappings to the observable space $\mathcal{S}^\eta \subset \mathbb{R}^d$, $M \leq d$. Then the distance in $\mathcal{S}^p$ (using local coordinates) can be approximated as:*

$$d(p, p')^2 := 2(\eta - \eta')^T \left[J_\varphi J_\varphi^T(\eta) + J_\varphi J_\varphi^T(\eta') \right]^{-1} (\eta - \eta'), \tag{3}$$

where J_φ is the Jacobian of the transformation. It holds

$$\|p - p'\|^2_{\mathbb{R}^M} = d(p, p')^2 + O(\|\eta - \eta'\|^4_{\mathbb{R}^d}). \tag{4}$$

The result also holds for the alternative approximation

$$d(p, p')^2 := \frac{1}{2}(\eta - \eta')^T \left[(J_\varphi J_\varphi^T)^{-1}(\eta) + (J_\varphi J_\varphi^T)^{-1}(\eta') \right] (\eta - \eta'). \tag{5}$$

Using the distance approximation (3) or (5), we define the density normalized weight matrix W_d

$$W_d := D_A^{-1/2} A D_A^{-1/2}, \quad \text{where} \quad A_{k,l} = \exp\left(-d\left(p^{(k)}, p^{(l)}\right)^2 / \epsilon \right), \tag{6}$$

with $D_A := \mathrm{diag}(A \cdot \mathbb{1})$ and $\mathbb{1}$ is the vector of all ones. Further, W_d can be transformed into

$$W_{rs} := D_d^{-1} W_d \quad \text{and} \quad W_s = D_d^{-1/2} W_d D_d^{-1/2}, \tag{7}$$

with $D_d := \mathrm{diag}(W_d \cdot \mathbb{1})$. The row stochastic matrix W_{rs} is similar to the symmetric matrix W_s in the sense that they share the same eigenvalues and, with ψ denoting an eigenvector of W_{rs} and ψ_s one of W_s, the corresponding eigenvectors are related by $\psi_s = D_d^{1/2}\psi$. See [Chu97] for more on spectral graph theory and normalized graph Laplacians.

It has been demonstrated in [SC08] that the discrete operator

$$L = W_{rs} - I, \tag{8}$$

for A as in (6), converges to a Fokker-Planck operator in the non-observable space $\mathcal{S}^p$

$$\mathcal{L}_{\mathcal{S}^p} f = \Delta f - \nabla U \cdot \nabla f, \text{ with } \quad U = -2 \log \mu, \tag{9}$$

where μ is the density of points in $\mathcal{S}^p$, which is (re)constructed from the density of data points in the observable space and the implicitly observed transformation φ. Therefore, through this construction we are approximating an operator in $\mathcal{S}^p$. Additionally, it has been demonstrated that, under suitable conditions, the eigenvector corresponding to the first non-trivial eigenvalue of the operator (8) is actually a function of the first non-observable variable, the second of the second variable, and so on, see [Sin06] for details.

As outlined we propose to use this setting for numerical simulations of a PDE model subject to parameter changes and other stochastic effects. To construct the discrete Fokker-Planck operator we take the nodes of a surface mesh K. We are considering a simulation bundle where each simulation is assumed to be obtained through a stochastic realization φ^i of a nonlinear transformation φ from a reference mesh. In this setting, a set of m simulations are available to us and based on this information we now can construct an operator which is invariant to the nonlinear transformation φ. One starts with a reference mesh and considers the simulation results at a time step as a cloud around each mesh point. Then from this cloud, the local sample covariance matrix $C^{(k)}$ is obtained and one approximates $J_\varphi(p^{(k)})J_\varphi^T(p^{(k)})$ and its inverse, in order to be able to evaluate expression (3) locally at each point $p^{(k)}$ of the reference simulation. In some sense we estimate the deterministic effect over the bundle of numerical simulations by this procedure. Most noteworthy, the obtained discrete Fokker-Planck operator can be considered to be invariant to the transformation φ, since we used a data-driven distance which is invariant to the deterministic effect, and therefore it is the same operator for all of the m surfaces stemming from the numerical simulations.

Algorithm 2 describes the general procedure for the evaluation of this operator.

Algorithm 2: Spectral decomposition of a discrete Fokker-Planck operator

Input: data set bundle $\{x^j\}, j = 1, \ldots, m$ of surfaces embedded in $\mathbb{R}^3$, where each x^j is given by N_h points $p^{j,(k)}$

Parameter: ϵ, n_{ev}

Output: first p eigenvectors of a discrete Fokker-Planck operator

foreach $k \in \{1, \ldots, N_h\}$ **do** ▷ `estimate local Jacobi matrices at` $p^{(k)}$

  $\mathbf{JJt}[k] =$ (pseudo)inverse of C_k, with C_k local sample covariance matrix from $p^{j,(k)}$

foreach $l, k \in \{1, \ldots, N_h\} \otimes \{1, \ldots, N_h\}$ **do** ▷ `calculate weight matrix`

  $\mathbf{A}[k, l] = \exp(-d(p^{(k)}, p^{(l)})^2/\epsilon)$, where $d(p^{(k)}, p^{(l)})$ after (3) and using $\mathbf{JJt}[k]$

compute W_{rs} and D_d using (6), (7) ▷ `density normal. row stoch. weight matrix`

solve $[\mathbf{U}, \mathbf{E}] = \text{eig}(W_{rs})$ ▷ `non-trivial eigenvectors`

return n_{ev} first non-trivial eigenvectors $D_d^{1/2}\mathbf{U}$

5 Decay of Spectral Coefficients and Separation of Effects

In general, using the eigenbasis of one of the introduced discrete operators and projecting mesh functions onto it is not necessarily beneficial as the number of projection coefficients is the same as the number of nodes on the mesh. We will now present numerical experiments to show that, first, projection coefficients do decay fast for real mesh functions and, second, that the

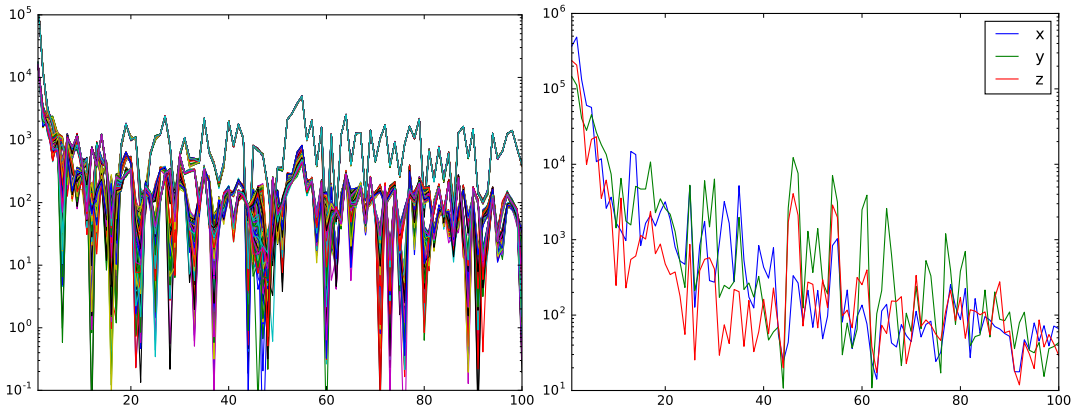

(a) magnitude of coefficients

(b) variance of coefficients

Figure 1: Magnitude and variance of the first 100 spectral projection coefficients for the mesh functions f_x^i, f_y^i, and f_z^i representing the deformation in a crash simulation, $i = 1, \ldots, 116$.

first eigenvectors do represent independent effects. An attempt to mathematically explain this behavior follows afterwards.

5.1 Empirical Observations for Numerical Simulation Bundles

As an illustrative example consider rotations, a distance preserving transformation. We assume a cylinder is discretized using a mesh and this object is then arbitrarily rotated. We use the Laplace-Beltrami operator as described in section 3, which is invariant to rotations. Now, consider mesh functions f_x^i, f_y^i, and f_z^i stemming from the i-th rotation, which for each mesh point have its resulting x, y, and z coordinate of the specific rotation as the function value, respectively. One can now observe that the first two coefficients are much bigger then the rest, and that the magnitude of the coefficients are further decreasing for higher eigenvectors. Now, if we take the spectral coefficients of the f_x^i, f_y^i, and f_z^i in regard to one of the eigenvectors and plot them for all rotations, where each point corresponds to one rotation f^i, we observe a sphere, unless the magnitude of the coefficients is very small. Furthermore, if we only consider rotations of the cylinder with respect to one axis, we observe a circle on the sphere, i.e. a rotational orbit. In the end, this is to be expected in this specific situation. With φ^i a rotation and f_x the x-coordinate of a mesh point, we can write $f_x^i = \varphi^i \cdot f_x$, and since the Laplace-Beltrami operator is invariant to a rotation we have $\mathcal{L} f_x^i = \varphi^i \mathcal{L} f_x$.

The next example is more realistic, taken from a numerical simulation of a car crash, where the simulation results are 3D deformations. We describe the setup in more detail in section 7.1, see also [BGIT+13]. The thickness values of parts of the car structure are varied to obtain 116 numerical simulations, then a structurally relevant part at a selected time step is chosen for the analysis. In figure 1a, projection coefficients for mesh functions f_x^i, f_y^i, and f_z^i, $i = 1, \ldots, 116$, using the basis from the discrete Fokker-Planck operator from section 3 are shown. It can be observed that the magnitude is largest in the first, say, 10 coefficients for all directions, afterwards only for the x component it stays larger. This can be explained by the translation of the car in x direction during the numerical crash simulation, here the biggest changes are taking place. Nevertheless, the variance is reduced for all 3 mesh functions, see figure 1b. Note also, that both magnitude and variance are correlated between all three directions, since the basis is computed

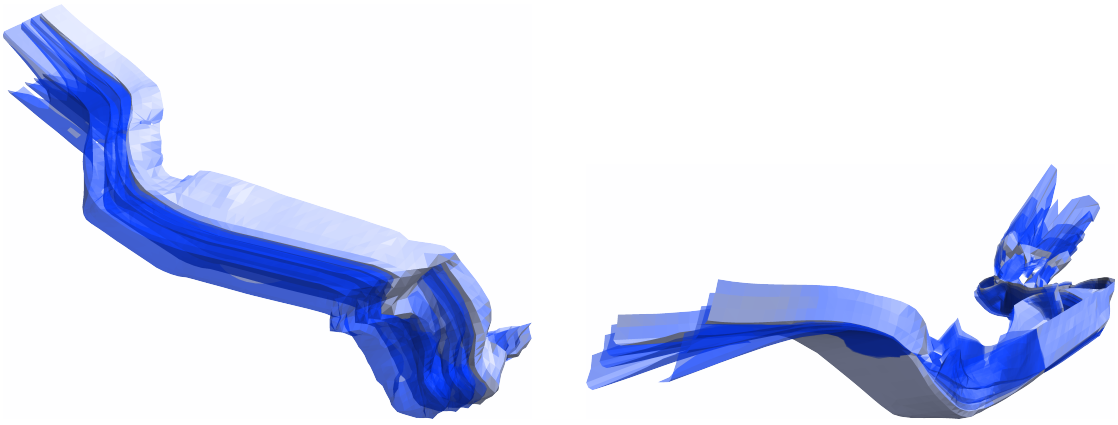

(a) translation (b) geometric deformation

Figure 2: Overlay of several reconstructions obtained when varying the coefficients with respect to the first and third component, respectively. A translation corresponds to the first eigenvector, while the third eigenvector reflects a geometric deformation.

from the joint mesh. One can use both, the magnitude and the variance to identify and threshold for the significant components in the spectral decomposition. Note that we observed a similar empirical decay behavior in other situations, including for the spectral coefficients arising in an airbag simulation, where even larger deformations take place.

In order to have a visual representation of the separation of effects by the spectral decomposition we reconstruct the deformed geometry as a linear combination of the eigenvectors. Here, we take the coefficients for the spectral components for the mesh functions f_x^j, f_y^j, and f_z^j of an arbitrarily chosen simulation j. We now vary the obtained spectral coefficient with respect to the first eigenvector. The result is shown in figure 2a, where we observe that the first component reflects a translation. In the same fashion, we can observe that the second corresponds to a rotation, the third to a global deformation, see Figure 2b, and the fourth to a local deformation, more details will be given in section 7.3.

The observed behavior of translation, rotation, and deformation gives numerical evidence that group actions can be represented by projections along eigenvectors of invariant operators. Quantifying the decay of the spectral coefficients as well being able to explain theoretically why using a discrete approximation of the Laplace-Beltrami operator or the Fokker-Planck operator allows such a decomposition into independent components, as observed in the numerical experiments, is an open problem, see [Iza17] for further exposition and first ideas in this direction. We propose in section 5.3 a conjecture for an explanation of the decay of the coefficients for the stochastic setting of the Fokker-Planck operator.

5.2 Discrete Orthogonal Decomposition

Once the eigenvectors ψ_j of some specific discrete operator are available, we can project any mesh function f^i defined on a mesh K^i along them and obtain as a result a set of spectral coefficients $\alpha_j^i, j = 1, \ldots, N_h$. The following expression is an analogue to the continuous case (1)

$$f^i = \sum_{j=1}^{N_h} \alpha_j^i \psi_j, \quad \alpha_j^i = \langle f^i, \psi_j \rangle, \tag{10}$$

where N_h corresponds to the number of nodes on the mesh K^i, which can be very large. Using a discrete operator, at least formally a large number of eigenvectors would be necessary to reconstruct a mesh function by its spectral coordinates.

Now assume K is a mesh which approximates a reference manifold $\mathcal{M}$ and let the mesh function $f : K \to \mathbb{R}$ be a function evaluated at the nodes of the mesh. Furthermore, let $\mathcal{M}^i, i = 1, \ldots, m$ be the manifolds obtained by the application of diffeomorphisms φ^i with corresponding approximations given by $\varphi^i_{|K^i}$ on the mesh K^i and let $f^i : K^i \to \mathbb{R}$ be mesh functions on K^i. It holds

Corollary 5.1. *Let an orthogonal basis $\{\psi_j\}_{j=1}^{N_h}$ consisting of N_h eigenvectors ψ_j be given, which is obtained from the spectral decomposition of a discrete approximation of either the Laplace-Beltrami operator after (2) or a Fokker-Planck operator after (8). Then all mesh functions f^i can be represented as*

$$f^i = \sum_{j=1}^{N_h} \alpha^i_j \psi_j, \tag{11}$$

where α^i_j are the spectral coefficients obtained by the projection of f^i into the eigenvector basis.

In our application setting, the functions $f^i : K^i \to \mathbb{R}^3$ would correspond to the x, y, and z components of a numerical solutions of a partial differential equation using the finite element method, as just before in section 5.1, i.e. we use the corollary for each component function of f^i.

5.3 Approximation Properties

As explained in the previous sections, we use operators that are invariant under a specific transformation. As a consequence we can project a set of mesh functions along the same basis for functions defined on a set of meshes. We now consider only the stochastic setting and will show, that under certain conditions one can expect a strong decay of the spectral coefficients depending on the smoothness properties of the data. In particular we conjecture an estimation that depends on the smoothness of the function and therefore, at least for a simplified setting, explains in parts the observed strong decay of the spectral coefficients.

Conjecture 5.2 (Decay of the Spectral Coefficients)**.** *Let the assumptions from section 4.2 hold and let the orthogonal decomposition based on a Fokker-Planck operator in corollary 5.1 be given. Then, for smooth functions $f^i : \mathcal{M}^i \to \mathbb{R}, f^i \in C^k, i = 1, \ldots, m$, the spectral coefficients $\alpha^i_j = \langle f^i|_K, \psi_j \rangle, j = 1, \ldots, N_h$ of their mesh representation $f^i|_K$ decay as*

$$|\alpha^i_j| \leq \frac{C}{(\gamma_j)^k} \|(f^i)^{(k)}\|_{L^2},$$

depending on the degree of smoothness k of the functions $f^i, i = 1, \ldots, m$, and $\gamma_{j+1} \geq \gamma_j$. The first eigenvectors recover the first independent components.

For a justification of this conjecture we employ the following observation from [Sin06].

Proposition 5.3. *Let the assumptions from section 4.2 hold. Given the eigenvalue problem (9) for the Fokker-Planck operator $\mathcal{L}_{\mathcal{S}^p}$, the operator can be separated as*

$$\mathcal{L}_{\mathcal{S}^p} = \sum_{l=1}^{d} \mathcal{L}_l,$$

where each $\mathcal{L}_l$ is a one-dimensional Fokker-Planck operator in an interval (a_l, b_l) with specific Neumann boundary conditions. The eigenfunctions of $\mathcal{L}_{\mathcal{S}_p}$ are tensor products of the one-dimensional eigenfunctions for the $\mathcal{L}_l$.

Note that the operator in expression (9) is the one on the unobservable manifold $\mathcal{S}^p$, which is assumed to be a subset of $\mathbb{R}^d$. The observable space is nonlinearly transformed, and we will approximate the operator in the observable space as detailed in section 3. Since the unobservable manifold on which we are considering the Fokker-Planck operator $\mathcal{L}$ is planar, the data density is a product of d one-dimensional densities, due to the assumed independence of the underlying Itô-processes. The full derivation can be found in [Sin06], see also [SC08, KHC12].

The following result is from the spectral approximation theory for Sturm-Liouville problems, see [CHQZ06, Chapter 5.2] for details.

Proposition 5.4. *Let $f \in C^k$, and its spectral coefficients $\hat{f}_j = \langle f, \hat{\psi}_j \rangle$, where $\hat{\psi}_j$, $j = \{0, 1, \dots, \}$ are the eigenfunctions of the Sturm-Liouville eigenvalue problem*

$$\frac{d}{dx}\left(e^{-U}\frac{d\hat{\psi}}{dx}\right) + \lambda e^{-U}\hat{\psi} = 0 \quad x \in (-1, 1), \tag{12}$$

with eigenvalue λ_j. Then the following holds,

$$|\hat{f}_j| \leq \frac{C}{(\lambda_j)^k}\|f^{(k)}\|_{L^2(-1,1)},$$

provided: p is zero at the boundary or the boundary conditions,

$$\alpha_1\hat{\psi}(-1) + \beta_1\hat{\psi}'(-1) = 0, \qquad \alpha_1^2 + \beta_1^2 \neq 0 \tag{13}$$

$$\alpha_2\hat{\psi}(1) + \beta_2\hat{\psi}'(1) = 0, \qquad \alpha_2^2 + \beta_2^2 \neq 0 \tag{14}$$

are satisfied.

Note that one often has $\lambda_j = \mathcal{O}(j^2)$, so that the denominator would be j^{2k}.

Justification of conjecture 5.2. We provide a sketch of a way to proof the conjecture. First, the decomposition in expression (11) is constructed using approximations of the eigenfunctions of the Fokker-Planck operator $\mathcal{L}_{\mathcal{S}_p}$ of independent stochastic Itô processes. In our case this operator can be separated into independent one-dimensional Sturm-Liouville problems due to proposition 5.3. Furthermore, as shown in [Sin06], the first eigenfunctions of the operator given in (9) provide the independent components and they correspond to the eigenfunctions of the Sturm-Liouville problem. Now, proposition 5.4 establishes an estimation of the decay rate of spectral coefficients, depending on the type of Sturm-Liouville problem and its boundary conditions. Assuming it can be applied in our setting, the decay of the spectral coefficients $\hat{f}_j^i, j = 1, \dots N_h$ with regard to the spectral decomposition of the one-dimensional components $\mathcal{L}_l$ from (5.3) can be approximated as

$$|\hat{f}_j^i| \leq \frac{C}{(\lambda_j^l)^k}\|(f^i)^{(k)}\|_{L^2},$$

depending on the degree of smoothness k of the functions $f^i, i = 1, \dots, m$. Suitably combining the bounds for the individual $\mathcal{L}_l$ one can achieve

$$|\hat{f}_j^i| \leq \frac{C}{(\gamma_j)^k}\|(f^i)^{(k)}\|_{L^2},$$

where the γ_j depends on the λ^ls.

Note that proposition 5.4 cannot be used directly here since only discrete data is available. How to formally bridge the gap between the analytical result and the discrete case is, to our knowledge, open. There are several recent works on point wise estimates between graph Laplacians and continuum operators or their spectral convergence, e.g. see the references in [TS17]. In [SW17] convergence of eigenvalues and eigenfunctions of graph Laplacians to those of a corresponding operator on the manifold in the limit of infinitely many independent random samples was shown in a unified framework. Furthermore, [TS17] show results using the variational convergence framework of Γ-convergence, and are also able to give rates for the convergence of the eigenvalues. Therefore, we deem it is reasonable to conjecture, that the outlined gap can be resolved in our setting built upon these works, although for eigenvectors and eigenprojections so far only consistency results exists to our knowledge. Additionally, approximation results for functions on a surface by a discrete function on a mesh are standard. By connecting these types of approximation results we conjecture that bounds on the spectral coefficients of discrete functions as above are attainable. □

We note that in the scope of the above results, the operator of independent components can be separated into independent eigenfunctions of 1D Sturm-Liouville problems, they are therefore ideal candidates as a basis for a set of simulations. Also the results show that at least for smooth functions, the decay of the first spectral coefficients can be high. For practical applications this is not necessarily the case since the mesh functions might not be smooth. Nevertheless for many real cases, relevant low dimensional information about the data sets can still be gained through the use of a single basis and the analysis of the first spectral coefficients.

6 Data Analysis Method

Based on the observed behavior and the theoretical considerations in section 5, we now propose an analysis method for data from numerical simulations, which involves a dimensionality reduction and a separation of effects along components.

6.1 Method Fundamentals

Given m simulations on a mesh with N_h nodes, we first compute a spectral decomposition of either the discrete Laplace-Beltrami operator with algorithm 1 or a discrete Fokker-Planck operator with algorithm 2. In a second step we select p eigenvectors for further analysis, e.g. by considering the decay of the eigenvalues of the operator or by looking at the variance of the spectral coefficients α^i of mesh functions f^i of particular interest.

Under certain conditions, as seen in section 5, the coefficients have a strong decay and therefore the "essential" part of a dataset is concentrated on a few coefficients. As will be seen in the applications, the first few components can correspond to the essential parts encoding the dominant behavior, and later ones become less relevant. At least for the Laplace-Beltrami operator they can be geometrically associated with high frequency parts or details [RBG+09]. As a consequence, depending on the decay of the coefficients, we are able to use only the first few spectral coordinates to analyze the main variability in the simulation data, see e.g. figure 1. Use of a single spectral basis for all simulations also naturally enables the construction of low dimensional representations for time dependent problems. Given a time dependent data set a projection of the mesh functions for all time steps into the same eigenbasis is possible.

Note that up to dimension 3 the projection coefficients can be used directly as embedding coordinates for visualization. If more coefficients are required to capture the data, a further

method of dimensionality reduction can be used to obtain an embedding. In particular, we use diffusion maps for further dimensionality reduction [CL06, BGIT+13, Iza14]. This method constructs a similarity matrix between the simulations based on their projection coordinates and uses the eigenvectors of this matrix, after a specific density-motivated normalization, to obtain low dimensional embedding coordinates.

The introduced data analysis procedure, which employs the eigenbasis of a chosen operator, has the following properties:

- a separation of independent effects in simulation data,
- an extraction of useful low dimensional information in the spectral coefficients of largest variation that allows to parameterize all simulation data,
- a natural simultaneous treatment of many time steps,
- simulations for a specific input parameter combination, not in the training set, can be approximated based on the given training data and embedding (projection) coordinates.

Some of these properties will be demonstrated in section 7 on realistic data.

Under the assumption that we are able to express all solutions of our differential equations (the simulations) as the action of some transformation from a reference configuration, we can think of the proposed method as one that approximates this group action, with the flexibility of being able to define the invariance property as needed. In particular we are often interested in mesh functions f_x, f_y, and f_z stemming from a numerical simulation, where for each mesh point the resulting x, y, and z coordinate at a time step of the simulation is the respective function value. For these particular mesh functions the assumed invariances or isometries would be (approximately) observed, which in parts explains the empirical results in the next section.

Note here, that our approach is related to nonlinear dimensionality reduction [LV07], in particular diffusion maps [CL06] and related ideas used in diffusion wavelets [CM06]. While these aproaches consider a manifold of general data points, we consider manifolds stemming from numerical simulations, which have additional structure in the form of isometries or invariances.

6.2 Comparison with Principal Component Analysis

Due to its simplicity and good properties, the PCA is likely the most employed method for dimensionality reduction. Given a dataset $X = \{X^1, X^2, \dots, X^m\}$, $X^i \in \mathbb{R}^n$ a very efficient way of representing the variability of the datasets is the PCA obtained from the eigenvalue decomposition given by $[US] = \mathrm{EVD}(X_c X_c^T)$, where X_c is a centered representation of X, U collects the eigenvectors, and S is a diagonal matrix whose diagonal elements are the eigenvalues. If the eigenvalues are ordered in descending order, then the first eigenvector corresponds to the first main variation of the dataset, the second to the second and so on. Often only a few coefficients are necessary to reconstruct each data so that $X^i \approx \sum_{k=1}^{p} \langle U_k, X^i \rangle U_k$ with $p < m \ll n$. The approach then reduces to the calculation of p eigenvectors. Note that underlying the PCA is the preservation of Euclidean distances in the high dimensional space [LV07] and that the embedding can also be computed by the singular valued decomposition of X_c, so that the computational effort scales mainly with the minimum of m and n.

In the case of numerical simulations in a finite element space, each simulation can be considered as a point in $\mathbb{R}^n, n = 3N_h$, where N_h is the number of nodes, in order to apply the PCA. Comparing the basis for the PCA, Laplace-Beltrami operator and the Fokker-Planck operator one observes significant differences. PCA can concentrate the variability of the data in just m coefficients, where m is the number of simulations available. The number of components for the

operators are bigger, namely as large as the number of nodes N_h, but the first coefficients are large in comparison with the rest. The latter is why we will use them for data analysis. For the PCA the first coefficients are related to the variability of the data, but not to a smooth part of the geometry nor any nonlinear component. While the first components of the PCA can encode much information, this is under the assumption that there is a linear transformation between high and low-dimensional space. If the data is on a nonlinear manifold or, in other words, if there is some nonlinear dependence on parameters, then other methods are needed. The operator approach suggested in this paper proposes a way to obtain the information about this low dimensional structures, we can decompose the data variability in a flexible way by changing the operator, which is constructed to preserve some quantity or property.

6.3 Operator Invariance Dependence

Taking a closer look at the proposed method, the important step is the construction of the discrete operator. For example pose invariance of a deformation can be achieved using an approximation of the Laplace-Beltrami operator constructed using geodesic distances in the finite element mesh. By (re)constructing a discrete Fokker-Planck operator in the specfied way, assuming an underlying stochastic Itô process, one can even obtain invariance to a nonlinear transformation. Assuming a decreasing order of the eigenvalues and a fast decay of the spectral coefficients, most of the "energy" of the data is concentrated in the first few components.

In the continuous case, it has been observed that the employed discrete Laplace-Beltrami operator has a discrete spectrum and that the eigenfunctions build a geometric decomposition of "frequencies" [RBG+09]. The proposed data analysis method has a flexible structure since one can influence what is considered a frequency, or component, through different distance measures on the mesh (or surface), which is related to the identification of the "correct" invariant operator corresponding to the way simulations are assumed or observed to behave under parameter changes.

Let us recall the invariance property for the investigated operators. For example, if they show only rigid changes (rotations or translations), then we can use the discrete Laplace-Beltrami operator L_K^h with the Euclidean distance since this operator is rotation and translation invariant. In the case of non-rigid transformations such as deformations that modify the shape arbitrarily, but do not tear or shrink the shape, we can use the Laplace-Beltrami operator precisely as defined in (2) using a geodesic distance approximated in the mesh by the graph distance. The operator constructed in this way will then be invariant to deformations that preserve geodesic distances. Finally, we could also have an arbitrary nonlinear transformation that brings one simulation to the next one in a stochastic setting, employing the Fokker-Planck operator as in (8) we can obtain an invariance to such a nonlinear transformation.

7 Data Analysis for Finite Element Simulation Bundles

Finite element simulations in industry are nowadays used to study the behavior of physical objects. Consider our running example of car parts under deformations due to a crash. The development of new car models demands the creation of many simulations with variations in material parameters or the geometry, which are analysed and modified based on engineering judgment in a time consuming research and development process. We propose now the application of the introduced data analysis method to such crash simulation results.

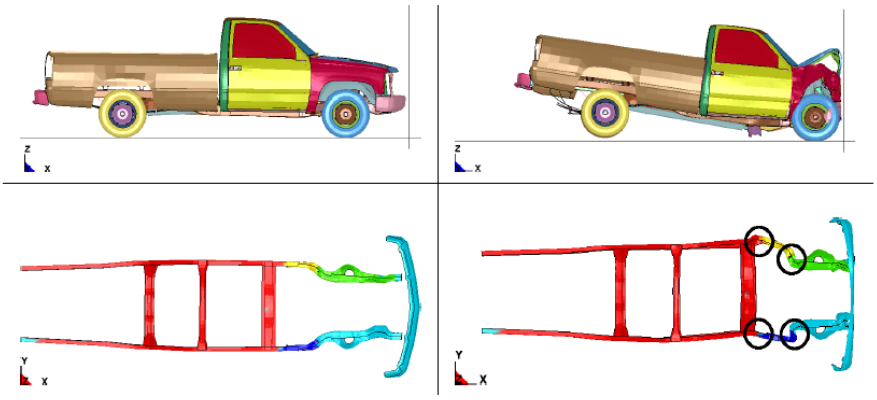

Figure 3: Exemplary frontal crash of the pick-up truck, shown with supporting structure.

7.1 Finite Element Signal Decomposition

First, we investigate the quality and properties of a representation of a function on a mesh stemming from crash simulations in the new basis. We consider a frontal crash simulation of a Chevrolet C2500 pick-up truck, a model with around 60,000 nodes from the National Crash Analysis Center[2]. We use 126 simulations[3] of a vehicle frontal crash where 9 part thicknesses are varied randomly by up to ±30%. The parts subject to thickness changes are shown in the lower part of figure 3.

The variation in the thickness of these 9 parts results in different deformations of the original structure, see also [BGIT+13]. The approximation of the Laplace-Beltrami operator using geodesic distances is calculated as described in section 4.1 using the initial mesh configuration. For any mesh function f the spectral coefficients with respect to the eigenvectors of the operator are then computed.

7.1.1 Decompositions of Deformation and Mesh Associated Variables

The deformations of the mesh for one simulation are now the considered mesh functions f_x^i, f_y^i and f_z^i, one for each coordinate x, y and z, i.e. 3 per simulation, respectively. Using the same connectivity of the original mesh, we can reconstruct the mesh deformations, separately for the x, y, and z coordinates, using $f^i = \sum_{j=1}^{p} \alpha_j^i \psi_j$ for several values of p.

From figure 4a, it can be clearly seen that using $p = 20$ only a very coarse approximation of the part can be reconstructed. Adding more values, e.g. $p = 100$, recovers more details of the part. It can also be clearly seen in figure 4b that most of the coefficients are small, with a few bigger ones. This is an essential feature which will be exploited for a classification task in section 7.1.2.

So far, we showed that the geometry of a car part can be represented using an orthogonal basis of the eigenvectors of an operator, by considering the x, y, z coordinates of each mesh point as three separate mesh functions. But, any function $f \in C^k(M)$ on the mesh can be represented by the linear combination of the eigenvectors. This implies that also other variables associated to each node can be represented using the same orthogonal basis, this can be used for variables

[2] `http://www.ncac.gwu.edu/vml/models.html`, accessible via `http://web.archive.org/`
[3] Computed with LS-DYNA `http://www.lstc.com/products/ls-dyna`

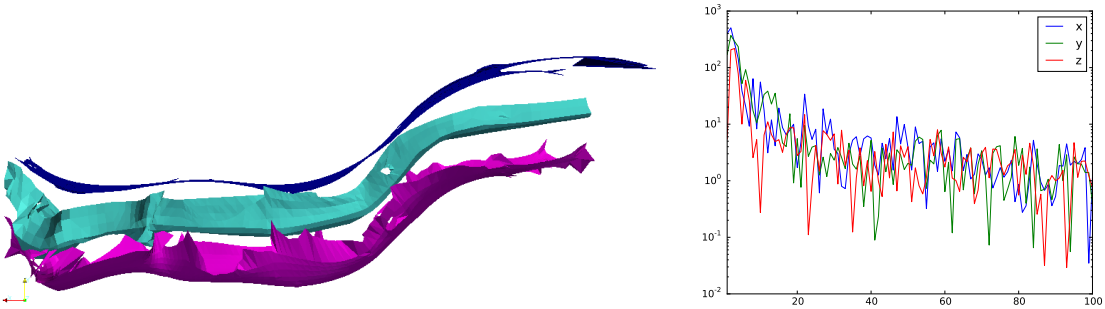

(a) Using the first p coefficients for the reconstruction, $p = 20$ coefficients (upper), $p = 100$ (lower) and original data (middle)

(b) Magnitude of spectral coefficients for x, y and z coordinates, respectively.

Figure 4: Analysis of a multi-scale reconstruction of a deformed shape.

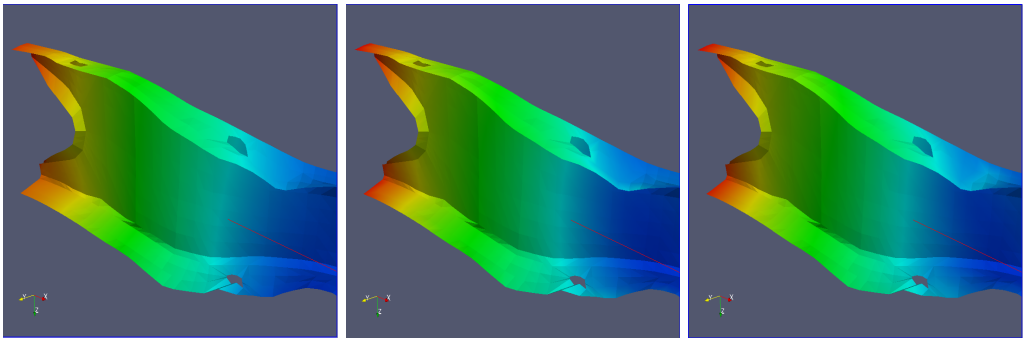

(a) $p = 20$ (b) $p = 200$ (c) original difference

Figure 5: Reconstruction of the differences between two time steps using p coefficients. The color coding represents the absolute difference of the movement of a given mesh point. For a qualitative data analysis one captures with $p = 20$ the essential behavior.

like nodal strains, temperatures, velocities, and so on.

We now demonstrate this with an example, where the nodal variable is the absolute difference of the movement of a mesh point between two time steps (6 and 7) of the car crash simulation. For figure 5 the difference is reconstructed using different values of p and it can be seen that with $p = 20$, compared with $p = 200$ and with the original data, almost the original color distribution is obtained for the nodal variable, i.e. for a qualitative analysis of the simulation results the first 20 coefficients capture the essential part of the behavior.

7.1.2 Data Analysis of Deformations in Crash Simulations

In [BGIT+13] on this data set nonlinear dimensionality reduction was investigated. There, the norm of the difference of the deformations between the two time steps 6 and 7 was used as the nodal value of the mesh function. A total of $m = 116$ simulations were used, where $f_k^i = \sqrt{\|u_k^i - v_k^i\|}$, with $u_k^i, v_k^i \in R^3, k = 1, \ldots, N_h = 1714$, and u_k^i, v_k^i denote the position of grid point k of simulation i at the time step 6 and 7, respectively. Based on this $m \times N_h$ dimensional data a lower-dimensional embedding was computed using diffusion maps, see [BGIT+13, Iza17]

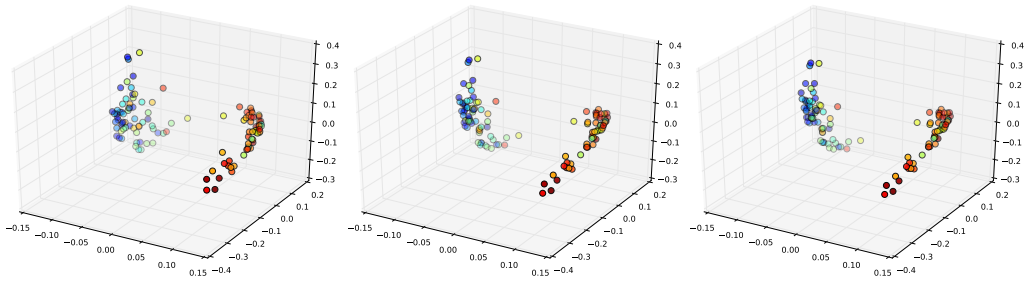

(a) $p = 4$ (b) $p = 20$ (c) raw data

Figure 6: Comparison of diffusion maps embeddings for the car crash data using different number of projection coefficients to the Laplace-Beltrami basis as feature vectors. The color of the points corresponds to the value of the thickness of one part which is varied for each simulation

for details. With this data analysis approach one was able to successfully identify buckling modes and input parameter dependences.

To demonstrate the usefulness of our approach we investigate the use of the spectral coefficients as input to the nonlinear dimensionality reduction procedure. We project as before all m vectors f^i along the eigenvectors of the approximation of the Laplace-Beltrami operator obtained in section 7.1. The result is a set of coefficients also in $\mathbb{R}^{N_h}$, where N_h is the number of nodes of the deformed beam. The coefficients decay very fast, i.e. similar to figure 4b, the energy of the signal is concentrated in very few coefficients and, as we presented in the theoretical part, one can equivalently use these coefficients instead of the original vectors of differences. Due to the decay, we just would like to keep the most significant ones and compare the embedding with diffusion maps using the first $p = 4$ and $p = 20$ coefficients with the embedding obtained using all the differences in $\mathbb{R}^{N_h}$. Figure 6 shows a comparison of these embeddings, where each point corresponds to the embedding of one f^i. The color of the points is given by the value of one of the varied plate thicknesses. It shows that this one has a high correlation with the resulting clustering of the deformation results and therefore graphically verifies the differences in the classification due to the eigenvectors.

It is interesting to see that with only $p = 4$ the structure of the embedding is almost the same and can be used for classification instead of using the original information of size $N_h = 1714$. This implies that the embedding is completely dominated by the first few components in the orthogonal decomposition, which correspond to coarse variations.

7.2 Time Dependent Analysis of Crash Simulations

Due to the use of a common basis for all simulations and time steps the introduced approach also allows an efficient analysis of time dependent information. Car crash simulations are strongly time dependent, in very few milliseconds the structure of a car can deform severely. Furthermore, an unstable behavior can originate from small variations in the material properties, initial load conditions, or numerically ill conditions. This phenomenon is called buckling and is a serious problem for the robust design of car components. Relevant for an engineer is not only the identification of principal bifurcation modes, but also the study of the starting point of the unstable behavior.

Our approach now allows a time dependent analysis of such unstable deformation characteristics. We use the same Chevrolet truck example as before, but to visualize the time dependent behavior we employ more time steps and therefore now use 167 simulations and 141 time steps,

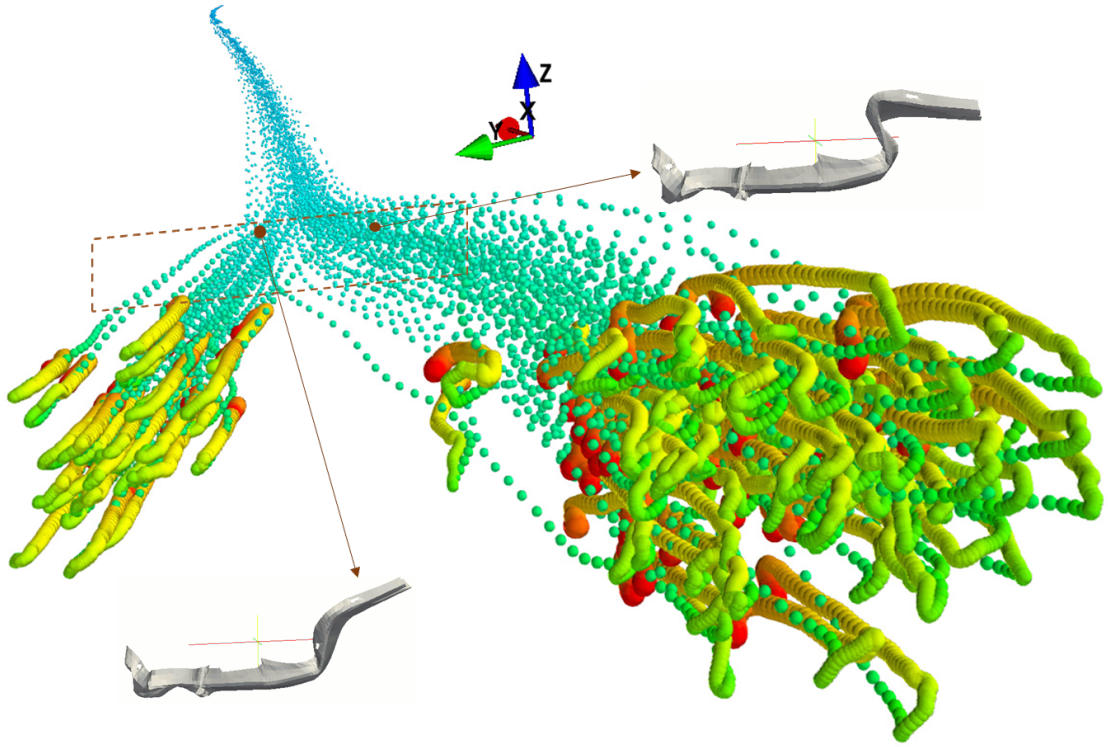

Figure 7: Reduced 3D representation of 23547 (167 simulations $\times$ 141 time steps) time dependent simulation results, obtained by the spectral decomposition of the Laplace-Beltrami operator. Each point indicates a simulation at a specific time. The coordinates are the first spectral coefficients of the mesh functions f_x^i, f_y^i, and f_z^i of each simulation at a time, i.e. for each direction x, y, and z of the movement of the car. They are colored according to the corresponding time step of the simulation. Two deformation modes are clearly visible, as well as the approximate time of the bifurcation.

where again 9 plate thicknesses are varied. Figure 7 shows an example where the deformation behavior over time for these simulations is displayed, where the color indicates the time. To obtain the shown 3D embedding we proceed along the lines of section 6 using the Laplace-Beltrami operator in algorithm 1 for the initial mesh. We use the obtained eigenvectors to project all simulations over all time steps by considering the mesh functions f_x^i, f_y^i, and f_z^i in time, representing the x, y, and z positions of each mesh point as before.

There are several observations that can be made from the obtained configuration in figure 7. We see that the reduced coordinates of the simulations give an organization of the data in time. A bifurcation clearly starts about half-way during the crash simulation, while one can see how the positions of the simulations for the last time steps appear mixed with those before. This corresponds with the rebound effect in a crash, where the car bounces back from the obstacle after the inertia of the movement was absorbed. The low dimensional representation shows two branches that corresponds to two different deformation modes of a car part as shown in figure 7.

Other embedding methods can be applied to the same data, but dealing with all time steps simultaneously is very limited. The usual approach is to use the PCA for time dependent analysis

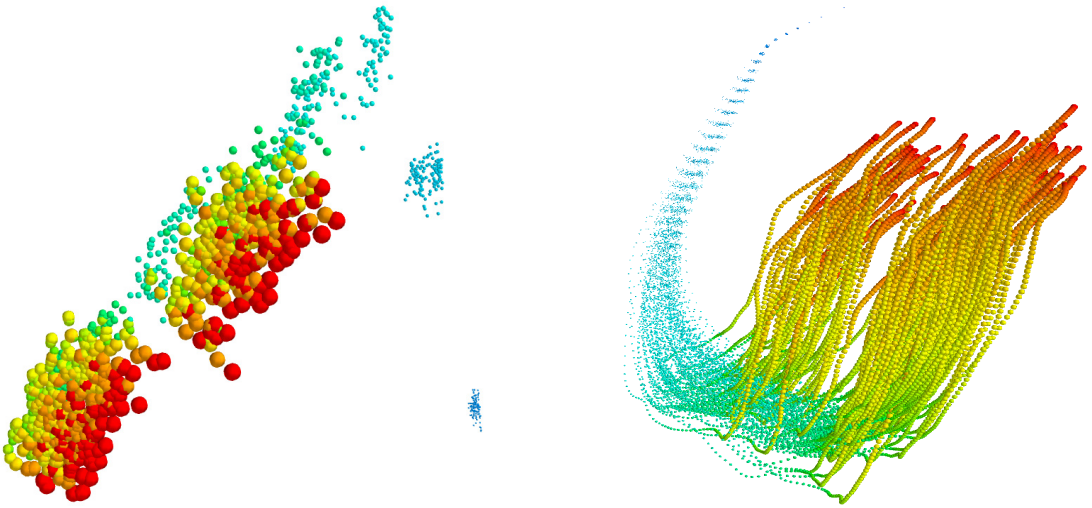

(a) Embedding using a PCA representation computed from one time step.

(b) Embedding using a PCA representation computed from all time steps.

Figure 8: Reduced 3D representation of simulations over several time steps, obtained with PCA. As before, the coordinates are the first spectral coefficients of the mesh functions f_x^i, f_y^i, and f_z^i of each simulation at a time. The points indicate a simulation at a specific time and are colored according to the corresponding time step of the simulation.

as well, so as a first try let us calculate a PCA using the data of all simulations from a time step where the bifurcation is clearly present. The spectral coefficients obtained by projecting the mesh functions f_x^i, f_y^i, and f_z^i for some selected time steps along these principal components gets the low dimensional structure shown in figure 8a, here again taking the first coefficient each. This approach does not produce adequate results since the variability over all time steps is not taken into account. Note that using other components of the PCA does not change this observation. Computing a PCA using all simulations and time steps does improve the results, but only to some degree, see figure 8b. Although a time behavior is now visible and a small separation is recognizable near the end, the clear separation and different results due to the bifurcation cannot be recognized in the embedding, in particular not the time of origin as is the case in figure 7.

Other nonlinear dimensionality reduction methods could in principle be used for dealing with this data set. But then, either the embedding method has to be computed as many times as time steps are available, where the switching of the eigenvectors makes recovering a time dependent low dimensional structure very cumbersome, if at all possible. Alternatively, one could attempt to embed other time steps into the coordinates obtained from one time step using the Nyström method, but this is as limited as the PCA example before. Using all simulations and all time steps is not feasible for spectral nonlinear dimensionality reduction approaches since one has to deal with large full matrices, and cannot go to a formulation in the size of the mesh, or relevant parts of it, as is possible for PCA or our approach.

7.3 Crash Modes

The deformations in a car crash are a complex mixture of different effects such as translations, rotations, local and global bending or torsion. How these interact, in particular in relation to the

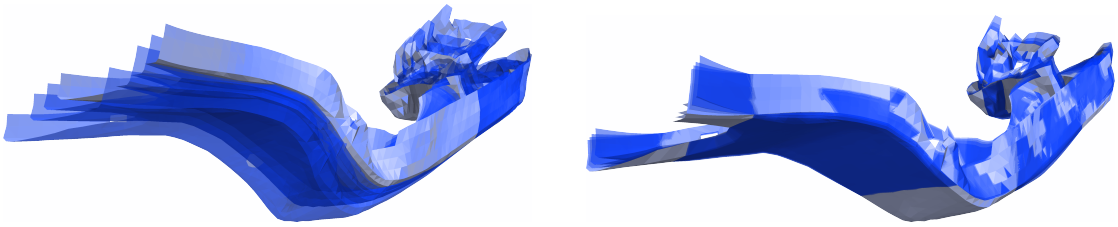

(a) rotation (b) local geometric deformation

Figure 9: Rotation and geometric deformations obtained when varying the coefficients with respect to the second and fourth component, respectively.

changes in the model design and material parameters is of great importance for the engineering analysis. Additionally, comparing simulations with experiments is a difficult and relevant task due to the variability of manufacturing parts, the material modeling and experimental conditions. Analyzing how the deformation differs between the real experiment and the numerical simulation is a mayor need in practice. Our approach turns out to be useful in addressing these challenges.

We use the same truck example as before, but we now study ways to identify and decompose different crash effects along so-called independent modes. We fix a specific time step (7 from 17) and evaluate for this shape the discrete Fokker-Planck operator. A total of 115 simulations are used, at each mesh point a cloud of 115 points is formed, that allows us to evaluate a local Jacobian, see algorithm 2. Our aim is to identify independent modes in the crash results. We consider the first $N_t = 4$ components of the orthogonal decomposition. A (re)construction of a (virtual) simulation reflecting only the transformations along a decomposition mode p can be done by fixing all the coefficients of the orthogonal decomposition with exception of the p-th one, i.e. the corresponding values for the other components stem from one chosen simulation, see also section 5.1.

A few reconstructed simulations for the first component, that is for $p = 1$, is shown in figure 2a. It can be seen that it corresponds to a translation. The obtained virtual simulations for $p = 2$ in figure 9a shows a rotation. For the third component with $p = 3$ we see in figure 2b a (global) deformation, while with $p = 4$ we obtain a different kind of (local) deformation, see figure 9b.

This example, as well as an extension of this procedure to morph simulations along some deformation modes, is described in detail in [Iza17]. The use of this approach for an alignment and comparison between time dependent numerical simulations and highly resolved 3D videos of real crash experiment is presented in [GIT17].

8 Summary and Discussion

The investigation of bundles of finite element simulations, e.g. for industrial engineering applications, is a challenge due to the high dimensionality and complexity of the data. We introduced an analysis approach that can cope with this problem, which is based on a new ansatz for low dimensional data representation. The method is based on the assumption that all simulations are related by transformations, in particular we propose a formulation in an abstract setting where all simulations are in the quotient space of all embeddings of a manifold in $\mathbb{R}^3$ modulo a transformation group. The simulations are then represented in a new basis derived from an operator invariant to a specific transformation group. It is shown theoretically that under certain conditions only few components in this new basis are required to recover the essential behavior

of the simulation data, which is also observed in examples with data stemming from engineering applications.

The presented applications of the new method show promising possibilities for the analysis of bundles of finite element simulation data. A more detailed presentation of our results is in [Iza17], which also contains additional applications as well as extensions of the methodology. Further research is warranted in order to analyze and to extend the assumptions of the theoretical setting, to analyze the use of operators invariant to other transformation, and also to extend the application areas of the analysis approach. For example, considerable efforts are invested in industrial product development for the determination of optimal designs in a global optimization approach, which is highly compute intensive due to the large amount of variables. We conjecture that the use of the new data representation has the potential to drastically reduce this complexity. In another context, we note that the reduced basis method (RBM) [QMN16] can be understood as a spectral method, where a problem dependent approximation basis is employed, which outlines a close relation to our approach. Initial investigations for using the basis computed by our approach in an RBM-context do look promising [Iza17].

From a theoretical point of view, we have proposed an abstract setting that incorporates the general framework of shape analysis for this type of datasets. Here, a link to the theoretical treatment of known results for the quotient $Emb(\mathcal{M}, \mathbb{R}^3)/Diff(\mathcal{M})$ is still missing. Further research has to be done, especially if one would like to efficiently evaluate geodesics in the obtained simulation spaces, similar as in the shape space setting.

Finally, the use of our approach in other industrial contexts is to be explored in detail. For example, we investigated the alignment of experimental measurement data in the form of point clouds from a real car crash in a crash facility with numerical simlation data. Here the aim is to find the corresponding numerical simulation to the measured point cloud data, for example to validate the numerical simulation approach or the involved material parameters. Such an alignment can be easier achieved in the eigenbasis obtained from a Fokker-Planck operator [GIT17].

Acknowledgements

The authors were supported within the projects SIMDATA-NL and VAVID funded by the German Federal Ministry of Education and Research (BMBF).

References

[AGHH08] S. Ackermann, L. Gaul, M. Hanss, and T. Hambrecht. Principal component analysis for detection of globally important input parameters in nonlinear finite element analysis. *IAM Institute of Applied and Experimental Mechanics, Stuttgart*, 2008.

[BBM14] M. Bauer, M. Bruveris, and P. W. Michor. Overview of the geometries of shape spaces and diffeomorphism groups. *J. Math. Imaging Vision*, 50(1-2):60–97, 2014.

[BCG05] M. Ben-Chen and C. Gotsman. On the optimality of spectral compression of mesh data. *ACM Trans. Graph*, 24:60–80, 2005.

[BGIT+13] B. Bohn, J. Garcke, R. Iza Teran, A. Paprotny, B. Peherstorfer, U. Schepsmeier, and C.-A. Thole. Analysis of car crash simulation data with nonlinear machine learning methods. In *ICCS 2013*, volume 18 of *Procedia Computer Science*, pages 621–630. Elsevier, 2013.

[BHM11] M. Bauer, P. Harms, and P. W. Michor. Sobolev metrics on shape space of surfaces. *Journal of Geometric Mechanics*, 3(4), 2011.

[BSW08] M. Belkin, J. Sun, and Y. Wang. Discrete Laplace operator on meshed surfaces. In *Proceedings of the Symposium on Computational Geometry*, SoCG '08, pages 278–287. ACM, 2008.

[CHQZ06] C. Canuto, M. Y. Hussaini, A. Quarteroni, and T. A. Zang. *Spectral Methods: Fundamentals in Single Domains*. Springer, 2006.

[Chu97] F. R. K. Chung. *Spectral Graph Theory*. American Mathematical Society, 1997.

[CL06] R. Coifman and S. Lafon. Diffusion maps. *Applied and Computational Harmonic Analysis*, 21(1):5–30, 2006.

[CM06] R. R. Coifman and M. Maggioni. Diffusion wavelets. *Applied and Computational Harmonic Analysis*, 21(1):53–94, 2006.

[CP94] S. Caddemi and M. D. Paola. Hysteretic systems subject to delta correlated input. In P. Spanos and Y. Wu, editors, *Probabilistic Structural Mechanics: Advances in Structural Reliability Methods*, pages 56–66. Springer, 1994.

[EK10] N. El Karoui. On information plus noise kernel random matrices. *Annals of Statistics*, 38(5):3191–3216, 2010.

[FJ07] P. T. Fletcher and S. Joshi. Riemannian geometry for the statistical analysis of diffusion tensor data. *Signal Processing*, 87:250–262, 2007.

[GIT17] J. Garcke and R. Iza-Teran. Machine learning approaches for data from car crashes and numerical car crash simulations. In *NAFEMS 2017, Stockholm*, 2017.

[HHM10] S. Huckemann, T. Hotz, and A. Munk. Intrinsic shape analysis: Geodesic PCA for Riemannian manifolds modulo isometric Lie group actions. *Statistica Sinica*, 20:1–100, 2010.

[Iza14] R. Iza Teran. Enabling the analysis of finite element simulation bundles. *International Journal for Uncertainty Quantification*, 4(2):95–110, 2014.

[Iza17] R. Iza Teran. *Geometrical Methods for the Analysis of Simulation Bundles*. Dissertation, Institut für Numerische Simulation, Universität Bonn, 2017.

[KBCL99] D. G. Kendall, D. Barden, T. K. Carne, and H. Le. *Shape and Shape Theory*. Wiley, 1999.

[KHC12] D. Kushnir, A. Haddad, and R. Coifman. Anisotropic diffusion on sub-manifolds with application to earth structure classification. *Applied and Computational Harmonic Analysis*, 32(2):280–294, 2012.

[LSLCO05] Y. Lipman, O. Sorkine, D. Levin, and D. Cohen-Or. Linear rotation-invariant coordinates for meshes. *ACM Trans. Graph.*, 24(3):479–487, 2005.

[LSS+10] R. Lai, Y. Shi, K. Scheibel, S. Fears, R. Woods, A. Toga, and T. Chan. Metric-induced optimal embedding for intrinsic 3d shape analysis. In *Computer Vision and Pattern Recognition (CVPR), 2010 IEEE Conference on*, pages 2871–2878, 2010.

[LV07] J. Lee and M. Verleysen. *Nonlinear Dimensionality Reduction*. Springer, 2007.

[Mic08] P. Michor. *Topics in Differential Geometry*. American Mathematical Society, 2008.

[MM06] P. W. Michor and D. Mumford. Riemannian geometries on spaces of plane curves. *J. Eur. Math. Soc.*, 8:1–48, 2006.

[MMAC09] R. Myers, D. Montgomery, and C. Anderson-Cook. *Response Surface Methodology: Process and Product Optimization Using Designed Experiments*. Wiley, 2009.

[MMP87] J. S. B. Mitchell, D. M. Mount, and C. H. Papadimitriou. The discrete geodesic problem. *SIAM J. Comput.*, 16(4):647–668, 1987.

[MT08] L. Mei and C.-A. Thole. Data analysis for parallel car-crash simulation results and model optimization. *Sim. Modelling Practice and Theory*, 16(3):329–337, 2008.

[OBCS+12] M. Ovsjanikov, M. Ben-Chen, J. Solomon, A. Butscher, and L. Guibas. Functional maps: A flexible representation of maps between shapes. *ACM Trans. Graph.*, 31(4):30:1–30:11, 2012.

[QMN16] A. Quarteroni, A. Manzoni, and F. Negri. *Reduced Basis Methods for Partial Differential Equations*. Springer, 2016.

[RBG+09] M. Reuter, S. Biasotti, D. Giorgi, G. Patanè, and M. Spagnuolo. Technical section: Discrete Laplace-Beltrami operators for shape analysis and segmentation. *Comput. Graph.*, 33(3):381–390, 2009.

[RWP06] M. Reuter, F. Wolter, and N. Peinecke. Laplace-Beltrami spectra as 'Shape-DNA' of surfaces and solids. *Computer-Aided Design*, 38(4):342–366, 2006.

[SC08] A. Singer and R. R. Coifman. Non-linear independent component analysis with diffusion maps. *Applied and Computational Harmonic Analysis*, 25(2):226–239, 2008.

[Sin06] A. Singer. Spectral independent component analysis. *Applied and Computational Harmonic Analysis*, 21(2):135–144, 2006.

[SJML05] A. Srivastava, S. Joshi, W. Mio, and X. Liu. Statistical shape anlaysis: Clustering, learning and testing. *IEEE Transactions on Pattern Analysis and Machine Intelligence*, 27:590–602, 2005.

[SW17] A. Singer and H.-T. Wu. Spectral convergence of the connection Laplacian from random samples. *Information and Inference*, 6(1):58–123, dec 2017.

[TNNC10] C. A. Thole, L. Nikitina, I. Nikitin, and T. Clees. Advanced mode analysis for crash simulation results. In *Proc. 9th LS-DYNA Forum*, 2010.

[TS17] N. G. Trillos and D. Slepčev. A variational approach to the consistency of spectral clustering. *Applied and Computational Harmonic Analysis*, 2017. to appear.